J. Fluid Mech. (1996), *vol.* 323, *pp.* 107–132

The linear stability of channel flow of fluid with temperature-dependent viscosity

By D. P. WALL AND S. K. WILSON

Department of Mathematics, University of Strathclyde, Livingstone Tower, 26 Richmond Street, Glasgow G1 1XH, UK

(Received 28 March 1995 and in revised form 5 March 1996)

The classical fourth-order Orr–Sommerfeld problem which arises from the study of the linear stability of channel flow of a viscous fluid is generalized to include the effects of a temperature-dependent fluid viscosity and heating of the channel walls. The resulting sixth-order eigenvalue problem is solved numerically using high-order finite-difference methods for four different viscosity models. It is found that temperature effects can have a significant influence on the stability of the flow. For all the viscosity models considered a non-uniform increase of the viscosity in the channel always stabilizes the flow whereas a non-uniform decrease of the viscosity in the channel may either destabilize or, more unexpectedly, stabilize the flow. In all the cases investigated the stability of the flow is found to be only weakly dependent on the value of the Péclet number. We discuss our results in terms of three physical effects, namely bulk effects, velocity-profile shape effects and thin-layer effects.

1. Introduction

A fundamental hydrodynamic stability problem is that of determining the stability of parallel viscous shear flow. One particular question, of great practical interest, is to determine the largest Reynolds number, R, at which channel flow of a viscous fluid may retain its steady laminar form. Applying linear stability theory to this problem yields the classical Orr–Sommerfeld equation derived by Orr (1907) and Sommerfeld (1908) which, together with the appropriate no-slip boundary conditions form a fourth-order eigenvalue problem. Although only a linear ordinary differential equation, the Orr–Sommerfeld equation has proved difficult to solve. Asymptotic solutions have been obtained by Heisenberg (1924), Tollmien (1929,1947) and Lin (1945*a*,*b*), and uniform asymptotic approximations have been obtained by Ng (1977) and Lakin, Ng & Reid (1978). Despite the difficulties caused by the stiffness of the Orr–Sommerfeld equation (for example, there are significant changes in the eigenfunctions near both walls and, for large R, in the vicinity of the critical layer), numerical solutions have been obtained using a variety of techniques by Kaplan (1964), Grosch & Salwen (1968), Gary & Helgason (1970), Orszag (1971) and Sloan (1977) among many others. The numerical results confirm the conclusions of the asymptotic analysis in identifying a finite critical Reynolds number, R_c, such that plane Poiseuille flow is linearly unstable to certain disturbances for $R > R_c$ and is linearly stable to all disturbances for $R < R_c$. If the maximum velocity and half the channel width are used as velocity and length scales respectively then Orszag's (1971) results yield $R_c \simeq 5772$.

The present work is concerned with generalizing the classical Orr–Sommerfeld problem to include the effects of a temperature-dependent fluid viscosity and heating of the channel walls. This problem was first addressed by Potter & Graber (1972) using a particular viscosity model relevant to water, but they neglected any disturbance to the basic-state temperature distribution and so obtained a modified fourth-order Orr–Sommerfeld equation which they solved numerically using Kaplan's (1964) filtering technique. In their study Potter & Graber (1972) held the temperatures of the channel walls fixed and restricted attention to when viscosity decreases as temperature increases. In this case they found a monotonic decreasing relationship of R_c with the temperature difference across the channel, finding, for instance, that a 78 K temperature difference between the channel walls approximately halved R_c. In the present work we examine the approximation adopted by Potter & Graber (1972). We find it to be exact when the Péclet number is zero and investigate its accuracy when the Péclet number is non-zero. Recently Schäfer & Herwig (1993) derived asymptotic equations for the present problem in the limit of a small non-dimensional viscosity gradient with respect to temperature which they solved numerically. At leading order they recovered the isothermal Orr–Sommerfeld equation and thermal effects entered at first order. They solved the leading-order problem using a shooting technique with Gram–Schmidt orthonormalization and the first-order problem using a multiple shooting method. These authors devoted most of their attention to the problem in which the heat flux is held constant on the channel walls, though they also presented some results for the problem in which the temperature of the channel walls is held constant in order to compare their results with those of Potter & Graber (1972). In this case Schäfer & Herwig found that R_c was a monotonically decreasing function of the temperature difference across the channel.

The present work investigates the linear stability of parallel shear flow of a fluid with temperature-dependent viscosity in a parallel-sided channel the walls of which are maintained at (different) constant temperatures. Numerical results are obtained using a high-order finite-difference method on an irregular grid with the resulting linear algebraic eigenvalue problem solved using the QZ matrix eigenvalue technique. In contrast to Potter & Graber (1972) a disturbance is permitted to the basic-state temperature distribution, while in contrast to Schäfer & Herwig (1993) the stability equations are solved non-asymptotically. Results for four different viscosity models are presented and discussed. It might be expected that heating, which causes viscosity to decrease throughout the channel, would always destabilize the flow; perhaps surprisingly this is not always found to be the case.

2. Governing equations

Adopting a Cartesian coordinate system whose origin is on the centreline of the channel with $x_2 = y$ the cross-channel ordinate and $x_1 = x$ parallel to the channel walls, we introduce the non-dimensional variables

$$\boldsymbol{x} = \frac{\boldsymbol{x}_*}{L}, \quad \boldsymbol{u} = \frac{\boldsymbol{u}_*}{V}, \quad p = \frac{p_*}{\rho V^2}, \quad t = t_* \frac{V}{L}, \quad \mu = \frac{\mu_*}{M}, \quad T = 2\left(\frac{T_* - T_l}{T_u - T_l}\right), \tag{2.1}$$

where L, ρ, T_u, T_l, M denote half the channel width, density, temperature at $y_* = L$, temperature at $y_* = -L$, and viscosity at $y_* = -L$ respectively;

$$V = \frac{JL^2}{2M} \tag{2.2}$$

where $-J$ ($J > 0$) is the constant imposed pressure gradient along the channel in the positive x-direction and $*$ denotes a dimensional quantity. The variables p, T, μ, t, $\boldsymbol{u} = (u_1, u_2, u_3) = (u, v, w)$ represent pressure, temperature, viscosity, time and velocity respectively. In the isothermal case V is the maximum velocity (or 3/2 times the average velocity) in the channel. The present non-dimensionalization differs from that used by Potter & Graber (1972) and Schäfer & Herwig (1993) who based their velocity scale, V_f, on the flux through the channel,

$$V_f = \frac{V}{2}\int_{-1}^{1} u(y)\mathrm{d}y. \tag{2.3}$$

Expressed in terms of these non-dimensional variables the governing Navier–Stokes and heat equations are given by

$$\frac{\partial u_i}{\partial t} + u_j\frac{\partial u_i}{\partial x_j} = -\frac{\partial p}{\partial x_i} + \frac{\mu}{R}\frac{\partial^2 u_i}{\partial x_j \partial x_j} + \frac{1}{R}\frac{\mathrm{d}\mu}{\mathrm{d}T}\frac{\partial T}{\partial x_j}\left(\frac{\partial u_i}{\partial x_j} + \frac{\partial u_j}{\partial x_i}\right), \tag{2.4a}$$

$$\frac{\partial u_j}{\partial x_j} = 0, \tag{2.4b}$$

$$\frac{\partial T}{\partial t} + u_j\frac{\partial T}{\partial x_j} = \frac{1}{P_e}\frac{\partial^2 T}{\partial x_i \partial x_i}, \tag{2.4c}$$

in which $\mu = \mu(T)$, $R = LV\rho/M$ is the Reynolds number and $P_e = RP_r$ is the Péclet number where $P_r = M/\rho\kappa$ is the Prandtl number. The appropriate non-dimensional boundary conditions representing no-slip and fixed temperature at the channel walls are

$$\boldsymbol{u}(y = \pm 1) = 0, \quad T(y = -1) = 0, \quad T(y = 1) = 2. \tag{2.5a–c}$$

3. Basic state

In this paper we consider the stability of a basic state in the form

$$\boldsymbol{u}(x, y, z, t) = (u_0(y), 0, 0), \quad p(x, y, z, t) = p_0(x), \quad T(x, y, z, t) = T_0(y). \tag{3.1}$$

Upon substituting into the governing equations (2.4) and boundary conditions (2.5) we obtain the basic-state equations

$$0 = -\frac{\mathrm{d}p_0}{\mathrm{d}x} + \frac{\mu}{R}\frac{\mathrm{d}^2 u_0}{\mathrm{d}y^2} + \frac{1}{R}\frac{\mathrm{d}\mu}{\mathrm{d}T_0}\frac{\mathrm{d}T_0}{\mathrm{d}y}\frac{\mathrm{d}u_0}{\mathrm{d}y}, \tag{3.2a}$$

$$0 = \frac{\mathrm{d}^2 T_0}{\mathrm{d}y^2}, \tag{3.2b}$$

subject to the boundary conditions

$$u_0(\pm 1) = 0, \quad T_0(-1) = 0, \quad T_0(1) = 2. \tag{3.3a–c}$$

Equation (3.2*b*) together with the boundary conditions (3.3*b*) and (3.3*c*) imply that $T_0(y) = 1 + y$, and so we are left to solve

$$R\frac{\mathrm{d}p_0}{\mathrm{d}x} = \frac{\mathrm{d}}{\mathrm{d}y}\left(\mu(T_0)\frac{\mathrm{d}u_0}{\mathrm{d}y}\right) = -2, \tag{3.4}$$

subject to boundary condition (3.3*a*). Any $\mu(T_0)$ and $u_0(y)$ which satisfy equation (3.4) subject to (3.3*a*) may be investigated. In the present work we shall consider the four specific viscosity/temperature relationships detailed below.

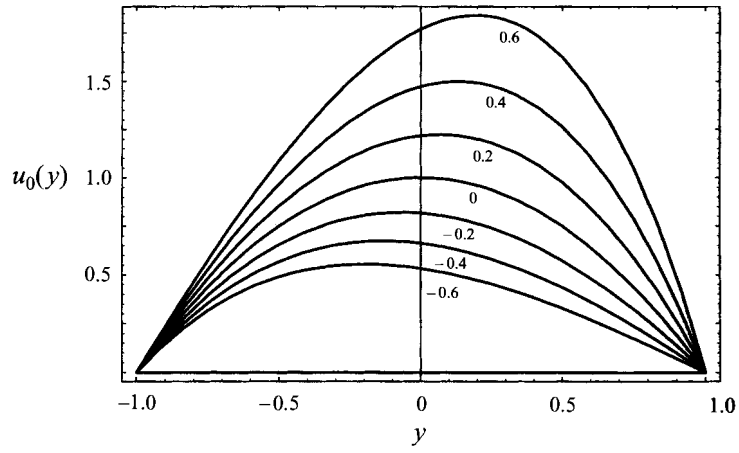

FIGURE 1. Basic-state velocity profiles $u_0(y)$ corresponding to the viscosity $\mu(T) = e^{-K_1 T}$ for the values of K_1 indicated.

3.1. *Model 1*

If we adopt the exponential viscosity/temperature relationship

$$\mu(T) = e^{-K_1 T} \tag{3.5}$$

then solving equation (3.4) for the velocity $u_0(y)$ yields

$$u_0(y) = -\frac{2}{K_1}\left[1 + \coth K_1 + (y - \coth K_1)e^{K_1(1+y)}\right]. \tag{3.6}$$

Velocity profiles for a number of different values of K_1 are plotted in figure 1.

3.2. *Model 2*

We also consider the linear viscosity/temperature relationship

$$\mu(T) = 1 - K_2 T \tag{3.7}$$

which requires $K_2 < 1/2$ in order for the viscosity to remain positive everywhere in the channel. The corresponding velocity is given by

$$u_0(y) = -\frac{2}{K_2}\left[\frac{-2\log\left[(1-2K_2)/(1-K_2(1+y))\right]}{\log(1-2K_2)} + 1 - y\right]. \tag{3.8}$$

These velocity profiles are qualitatively similar to those in figure 1.

3.3. *Model 3*

The results obtained for the viscosity models 1 and 2 suggested that it would be interesting to investigate a viscosity/temperature relationship for which the viscosity falls more rapidly near the hot wall ($y = 1$) than in the rest of the channel as the temperature increases. Accordingly we also consider the viscosity/temperature relationship

$$\mu(T) = 1 + b(1 - e^{K_3 T}) \tag{3.9}$$

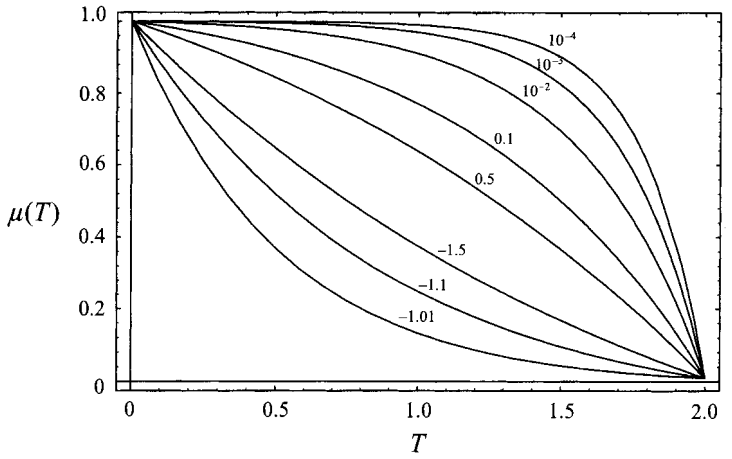

FIGURE 2. The viscosity relationship $\mu(T) = 1 + b(1 - e^{K_3 T})$ when K_3 is chosen so that $\mu(2) = 0.01$ for the values of b indicated.

in which, unless otherwise stated, we will assume that $b > 0$. In order for the viscosity to remain positive everywhere in the channel we require that

$$K_3 < \frac{1}{2}\log\left(1 + \frac{1}{b}\right) = \hat{K}_3. \tag{3.10}$$

For reference we plot a selection of these viscosity/temperature relationships in figure 2. Note that when $K_3 < 0$ then $1 \leqslant \mu(T) < 1 + b$ and hence $\mu(T)$ tends uniformly to 1 as $b \to 0$. However, when $K_3 > 0$ we can always make $\mu(2)$ as small as we choose by selecting K_3 sufficiently close to $\hat{K}_3$ for any value of b, with, as shown in figure 2, a less viscous layer near $y = 1$ becoming more prominent as $b \to 0$. We also note that, for a given value of b, $\mu(T) \to 1 + b$ as $K_3 \to -\infty$ if $T > 0$, but with $\mu(0) = 1$. The corresponding velocity is given by

$$\begin{aligned} u_0(y) = -\gamma y^2 + \frac{2\gamma y}{K_3}\log(1 - b\gamma e^{K_3(1+y)}) + \frac{2\gamma}{K_3^2}\mathrm{Li}_2(b\gamma e^{K_3(1+y)}) \\ + D\gamma\left[y - \frac{1}{K_3}\log\left(1 + b[1 - e^{K_3(1+y)}]\right)\right] + E, \end{aligned} \tag{3.11}$$

where we have written $\gamma = (1 + b)^{-1}$ and introduced

$$D = \frac{2\left(\mathrm{Li}_2(b\gamma) - \mathrm{Li}_2(b\gamma e^{2K_3}) - K_3\log[\gamma(1 - b\gamma e^{2K_3})]\right)}{K_3\left(2K_3 - \log[1 + b(1 - e^{2K_3})]\right)},$$

$$E = \gamma\left(1 + \frac{2}{K_3^2}[K_3\log\gamma - \mathrm{Li}_2(b\gamma)] + D\right)$$

and where

$$\mathrm{Li}_2(z) = \int_z^0 \frac{\log(1 - t)}{t}\mathrm{d}t = \sum_{k=1}^{\infty}\frac{z^k}{k^2}$$

is the second polylogarithmic function. When $K_3 > 0$, and also for $K_3 < 0$ when $|K_3|$ is sufficiently small, velocity profiles are again qualitatively similar to those plotted in figure 1. Otherwise, it is easily found that

$$\lim_{K_3 \to -\infty} u_0(y) = \frac{1}{1+b}(1-y^2), \tag{3.12}$$

so that the velocity profile is ultimately symmetrical as $K_3 \to -\infty$.

3.4. *Model 4*

To facilitate comparison with the previous investigation performed by Potter & Graber (1972) we also use the non-dimensional viscosity/temperature relationship given by

$$\mu(T) = Ce^{(K_4 T+F)^{-1}} \tag{3.13}$$

which has been proposed as a model for the viscosity for water. In the numerical calculations we fix the value of $F = 0.16393$ which in turn fixes $1/C = 445.9$ and vary K_4 in order to permit comparison with the results of Potter & Graber. The corresponding velocity is given by

$$u_0(y) = -\frac{2}{K_4^2 C}\left[\Gamma(-2, [K_4(1+y)+F]^{-1}, F^{-1}) - H\,\Gamma(-1, [K_4(1+y)+F]^{-1}, F^{-1})\right], \tag{3.14}$$

where we have introduced the constant

$$H = \frac{\Gamma(-2, [2K_4+F]^{-1}, F^{-1})}{\Gamma(-1, [2K_4+F]^{-1}, F^{-1})}$$

and where

$$\Gamma(a, z_0, z_1) = \int_{z_0}^{z_1} e^{-t} t^{a-1} dt$$

is the generalized Gamma function. These velocity profiles are again qualitatively similar to those in figure 1.

4. Linear stability

In accordance with classical linear stability theory we seek solutions in the form $u = u_0(y) + u_1(x, y, z, t)$ with similar expressions for v, w, p and T, where the perturbation is assumed to have the normal mode form

$$u_1 = \hat{u}(y)e^{i(\alpha x+\beta z-\alpha\sigma t)}, \tag{4.1}$$

with similar expressions for v_1, w_1, p_1 and T_1. The wavenumbers α and β are required to be real in order that the disturbance remains bounded as $x, z \to \pm\infty$. Thus the growth (or decay) rate of a given mode is given by $\alpha\sigma_i$ where σ_i is the imaginary part of the eigenvalue σ, and the mode will grow exponentially in

time if $\alpha\sigma_i > 0$ and will decay exponentially if $\alpha\sigma_i < 0$. We determine the linear stability of the flow by selecting the mode with the largest growth rate; should this be positive the flow is unstable, should it be negative the flow is stable. If the growth rate is zero the flow is neutrally stable. Substituting into the governing equations (2.4) and neglecting second- and higher-order products of the perturbations we obtain

$$-\mathrm{i}\alpha\hat{u}(\sigma - u_0) + \hat{v}u_0' = -\mathrm{i}\alpha\hat{p} + \frac{1}{R}(\mu(T_0)[\hat{u}'' - (\alpha^2 + \beta^2)\hat{u}] + \hat{T}\mu'(T_0)u_0'') + \frac{1}{R}\hat{T}\mu''(T_0)T_0'u_0' + \frac{1}{R}\mu'(T_0)(T_0'\hat{u}' + \hat{T}'u_0' + \mathrm{i}\alpha\hat{v}T_0'), \quad (4.2a)$$

$$-\mathrm{i}\alpha\hat{v}(\sigma - u_0) = -\hat{p}' + \frac{1}{R}\mu(T_0)[\hat{v}'' - (\alpha^2 + \beta^2)\hat{v}] + \frac{1}{R}\mu'(T_0)(2T_0'\hat{v}' + \mathrm{i}\alpha\hat{T}u_0'), \quad (4.2b)$$

$$-\mathrm{i}\alpha\hat{w}(\sigma - u_0) = -\mathrm{i}\beta\hat{p} + \frac{1}{R}\mu(T_0)[\hat{w}'' - (\alpha^2 + \beta^2)\hat{w}] + \frac{1}{R}\mu'(T_0)T_0'(\hat{w}' + \mathrm{i}\beta\hat{v}), \quad (4.2c)$$

$$\mathrm{i}\alpha\hat{u} + \hat{v}' + \mathrm{i}\beta\hat{w} = 0, \quad (4.2d)$$

$$-\mathrm{i}\alpha\hat{T}(\sigma - u_0) + \hat{v}T_0' = \frac{1}{P_e}[\hat{T}'' - (\alpha^2 + \beta^2)\hat{T}], \quad (4.2e)$$

where a prime denotes differentiation. The above normal mode perturbation equations are subject to the boundary conditions

$$\hat{u} = \hat{v} = \hat{w} = \hat{T} = 0 \quad (4.3)$$

at $y = \pm 1$ and form an eigenvalue problem whose solution can be expressed in the form $\sigma = \sigma(\alpha, \beta, R, P_e)$. As in the isothermal case we may now make use of Squire's theorem (see Squire 1933) which ensures that it is sufficient to consider two-dimensional disturbances for which the perturbation equations may be obtained from equations (4.2) by setting $\beta = \hat{w} = 0$. Details of Squire's theorem applied to the present non-isothermal problem are given by Wall (1996). Without loss of generality we take $\alpha \geqslant 0$ and so a given mode is unstable if $\sigma_i > 0$, stable if $\sigma_i < 0$ and neutrally stable if $\sigma_i = 0$.

Since we are now only considering a two-dimensional disturbance it is convenient to introduce a stream function for the perturbation velocity,

$$\Psi(x, y, t) = \hat{\psi}(y)\mathrm{e}^{\mathrm{i}\alpha(x - \sigma t)} \quad (4.4)$$

defined in the usual way ($\hat{u} = \hat{\psi}'$, $\hat{v} = -\mathrm{i}\alpha\hat{\psi}$), so that the incompressibility condition (4.2*d*) is automatically satisfied. Upon differentiating equation (4.2*a*) with respect to y and substituting in (4.2*b*) for p' we obtain the thermal Orr–Sommerfeld equations

$$\frac{\mathrm{i}}{R}\left[\mu(T_0)(\psi^{(4)} - 2\alpha^2\psi'' + \alpha^4\psi) + \mu'(T_0)(\mathrm{D}_1\psi + \mathrm{E}_1 T) + \mu''(T_0)(\mathrm{D}_2\psi + \mathrm{E}_2 T) + \mu'''(T_0)u_0'T_0'^2T\right] = \alpha(\sigma - u_0)(\psi'' - \alpha^2\psi) + \alpha\psi u_0'', \quad (4.5)$$

$$\mathrm{i}\alpha(u_0 - \sigma)T - \mathrm{i}\alpha T_0'\psi = \frac{1}{P_e}(T'' - \alpha^2 T), \quad (4.6)$$

subject to the boundary conditions

$$\psi(\pm 1) = 0, \ \psi'(\pm 1) = 0, \ T(\pm 1) = 0, \quad (4.7)$$

where we have introduced the operators

$$\mathrm{D}_1 = 2T_0'\left(\frac{\mathrm{d}^3}{\mathrm{d}y^3} - \alpha^2\frac{\mathrm{d}}{\mathrm{d}y}\right) + T_0''\left(\frac{\mathrm{d}^2}{\mathrm{d}y^2} + \alpha^2\right), \tag{4.8a}$$

$$\mathrm{E}_1 = u_0'\frac{\mathrm{d}^2}{\mathrm{d}y^2} + 2u_0''\frac{\mathrm{d}}{\mathrm{d}y} + (\alpha^2 u_0' + u_0'''), \tag{4.8b}$$

$$\mathrm{D}_2 = T_0'^2\left(\frac{\mathrm{d}^2}{\mathrm{d}y^2} + \alpha^2\right), \tag{4.8c}$$

$$\mathrm{E}_2 = 2u_0'\,T_0'\frac{\mathrm{d}}{\mathrm{d}y} + (2T_0'\,u_0'' + u_0'\,T_0''), \tag{4.8d}$$

and have dropped the hats for clarity. The equations (4.5) and (4.6) together with the boundary conditions (4.7) form a sixth-order eigenvalue problem for σ as a function of α, R and P_e. Note that in the special case $T \equiv 0$, $\mu \equiv 1$ we recover the familiar fourth-order isothermal Orr–Sommerfeld problem.

5. Computational details

5.1. *Numerical method*

The numerical method used in the present work is an extension of Gary & Helgason's (1970) finite-difference technique for solving an eigenvalue problem posed by a single linear ordinary differential equation (with appropriate boundary conditions) to solve n coupled linear equations in θ_j, $j = 1,\ldots,n$, where in the present application $n = 2$. Details of this numerical technique are given by Wall (1996). A FORTRAN code was written to solve this eigenvalue problem using a finite-difference method and is capable of adopting arbitrary-order approximations for any order of derivative appearing in either the equations or the boundary conditions limited only by the number of grid points, $N+1$, used. We can adjust the number of stencil points used at external nodes if we wish to increase, decrease or maintain the order of approximation there. Such flexibility demands an efficient algorithm for calculating finite-difference weights and this was accomplished using the notably short and fast algorithm recently discovered by Fornberg (1988). For a given (not necessarily regular) set of grid points $\{x_0,\ldots,x_N\}$, the point at which approximations are required $x = \xi$ (not necessarily a grid point) and highest order of derivative of interest, m, Fornberg's algorithm determines weights d_{ij}^k such that the approximations

$$\left.\frac{\partial^k f}{\partial x^k}\right|_{x=\xi} \simeq \sum_{j=0}^{i} d_{ij}^k f(x_j) \quad \text{for } k = 0,\ldots,m,\ i = k,\ldots,N \tag{5.1}$$

are all optimal in the sense that they permit the maximum order of approximation possible for a stencil consisting of $i+1$ points (indeed for the case $m = 0$ this algorithm offers the fastest way known to perform polynomial interpolation at a single point). After discretization we require the solution of a generalized linear algebraic eigenvalue problem in the form $\boldsymbol{A\theta} = \lambda\boldsymbol{B\theta}$, where $\boldsymbol{A}$ and $\boldsymbol{B}$ are $n(N+1)$th-order square matrices, $\boldsymbol{\theta} = (\theta_{10},\theta_{11},\ldots,\theta_{1N},\theta_{20},\ldots,\theta_{2N},\ldots\ \ldots,\theta_{n0},\ldots,\theta_{nN})^T$ where θ_{ji} represents our approximation to $\theta_j(x_i)$ for $j = 1,\ldots,n$, $i = 0,\ldots,N$ and λ is the corresponding eigenvalue of the system. We solve for the eigenvalues (and eigenvectors if required) using the QZ algorithm described, for example, by Wilkinson (1979) and implemented using the NAG routine F02GJF. One facet of this method is that there

K_2	s_0
0.46	14
0.47	17
0.475	25
0.48	34

TABLE 1. Optimum stretching parameters s_0 for the linear viscosity relation $\mu(T) = 1 - K_2 T$ as $K_2 \to 1/2$.

is no distinction in terms of computational cost between full and non-full matrices so there is no additional cost in adopting high-order finite-difference methods. The computational cost of the QZ algorithm is $O(N_{A,B}{}^3)$ where $N_{A,B}$ is the order of the matrices $\boldsymbol{A}$ and $\boldsymbol{B}$ and since in practice the majority of the runtime is taken up by the QZ algorithm rather than obtaining the matrices $\boldsymbol{A}$ and $\boldsymbol{B}$ doubling the number of grid points used approximately octuples the runtime of the code. The code was initially successfully tested on several test problems with known analytical or numerical solutions; details are again given by Wall (1996).

To obtain the numerical results presented in the present work we adopted the same order of approximation, J, for all the derivatives and found that in most cases an approximate empirical rule for the optimum value of J was

$$J = \frac{N}{10} + 2. \tag{5.2}$$

The problem was solved on an irregular grid x_i for $i = 0, \ldots, N$, which was obtained from the regular grid s_i for $i = 0, \ldots, N$ (where $s_0 = 0$ and $s_N = 1$) through application of the mapping

$$x_i = 2X(s_i) - 1 \text{ for } i = 0, \ldots, N, \tag{5.3}$$

where

$$X(u) = \frac{1}{2} + \frac{\tanh[(u - 1/2)C]}{2 \tanh C/2}, \tag{5.4}$$

is Vinokur's (1983) antisymmetric stretching function which clusters points away from the centre of the channel and towards the critical layers and the channel walls. The slope parameter

$$s_0 = \left.\frac{\mathrm{d}X}{\mathrm{d}u}\right|_{u=0} = \left.\frac{\mathrm{d}X}{\mathrm{d}u}\right|_{u=1} = \frac{C}{\sinh C} \tag{5.5}$$

is chosen by the user. The value $s_0 = 4.5$, an optimum choice for solving the isothermal problem on the whole channel, was used as a starting point for non-isothermal calculations and was adjusted as it became necessary. In particular for viscosity model 2 as $K_2 \to 1/2$ and model 3 as $K_3 \to \hat{K}_3$ the eigenfunctions undergo rapid change near the hot wall $y = 1$ and this necessitated increasing the value of s_0; values of s_0 used for model 2 as $K_2 \to 1/2$ are given in table 1.

For a given temperature/viscosity relationship and value of P_e we can calculate the (discrete) eigenvalue spectrum for σ at each point in the (R, α)-plane. Ordering the spectrum of eigenvalues according to

$$\sigma_i^{(1)} > \sigma_i^{(2)} > \sigma_i^{(3)} > \ldots$$

we define the point (R, α) to be stable if $\sigma_i^{(1)} < 0$, unstable if $\sigma_i^{(1)} > 0$ and neutrally

stable if $\sigma_i^{(1)} = 0$. Calculations were made on a DEC 3400S mainframe computer and to perform one evaluation of the σ-spectrum took around 15 s for $N = 100$ and $J = 12$ if eigenvectors were not simultaneously calculated and around 30 s if they were.

5.2. *Marginal stability curve and critical-point calculation*

In order to determine the stability of the flow we need to calculate the marginal stability curve in the (R, α)-plane on which $\sigma_i^{(1)} = 0$ which separates stable from unstable regions. For a given viscosity model and value of P_e this is accomplished through use of the van Wijngaarden–Dekker–Brent root-finding method described in Brent (1973). We iterate towards the marginal Reynolds number, R_m, for fixed α on the lower branch of the marginal stability curve and because the upper branches of the marginal stability curves are typically fairly flat it was found to be more convenient to iterate towards the marginal wavenumber, α_m, for fixed R on the upper branch. On each curve we may further identify the critical Reynolds number, R_c, which is the global minimum of the marginal stability curve with respect to R. The value of R_c is of prime importance since any flow with $R < R_c$ is linearly stable to all disturbances whilst for $R > R_c$ there exist disturbances to which the basic state is unstable. We denote the values of α and σ when $R = R_c$ by α_c and σ_c respectively with the latter, of course, being real since the critical point lies on the marginal stability curve. We calculate $(R_c, \alpha_c, \sigma_c)$ through use of Brent's (1973) minimization algorithm applied to minimizing $R_m(\alpha)$ in conjunction, of course, with the van Wijngaarden–Dekker–Brent root-finding method to iterate to the value of $R_m(\alpha_p)$ corresponding to each successive estimate α_p of α_c. In most cases $N = 80$ together with a fractional tolerance for α_c of 0.1% was sufficient to find R_c to within 0.01% when an absolute tolerance of ± 0.1 was used in finding each R_m. In practice, of the three values $(R_c, \alpha_c, \sigma_c)$, usually α_c was the slowest to converge and a larger value of N was sometimes required to obtain accurate values for this quantity. A larger value of N was also required for viscosity models 2 as $K_2 \to 1/2$ and model 3 as $K_3 \to \hat{K}_3$ since in these limits the rates of change of the respective eigenfunctions become very large near the hot wall ($y = 1$).

6. Results

In this section we present solutions of the thermal Orr–Sommerfeld problem given by equations (4.5) and (4.6) subject to (4.7) for the four viscosity models described by equations (3.5), (3.7), (3.9) and (3.13). Further details, including marginal stability curves, values of σ on the marginal curves and critical eigenfunctions for all four viscosity models are given by Wall (1996). For all four viscosity models considered here, the stability characteristics of the respective basic-state flows were found to be only very weakly dependent on the value of P_e. Since all the results obtained by varying P_e are qualitatively similar, in most cases we present results only for $P_e = 1$. When $K_1 = K_2 = K_4 = K_3 = 0$ we recover the isothermal Orr–Sommerfeld problem for plane Poiseuille flow where $\mu \equiv 1$ for which we obtain

$$(R_c^0, \alpha_c^0, \sigma_c^0) = (5772.2218, 1.020547, 0.2640003)$$

with $N = 120$ and $J = 14$ (converged to the figures quoted) in excellent agreement with earlier authors, for example the results obtained using a shooting method by Davey quoted in Drazin & Reid (1981).

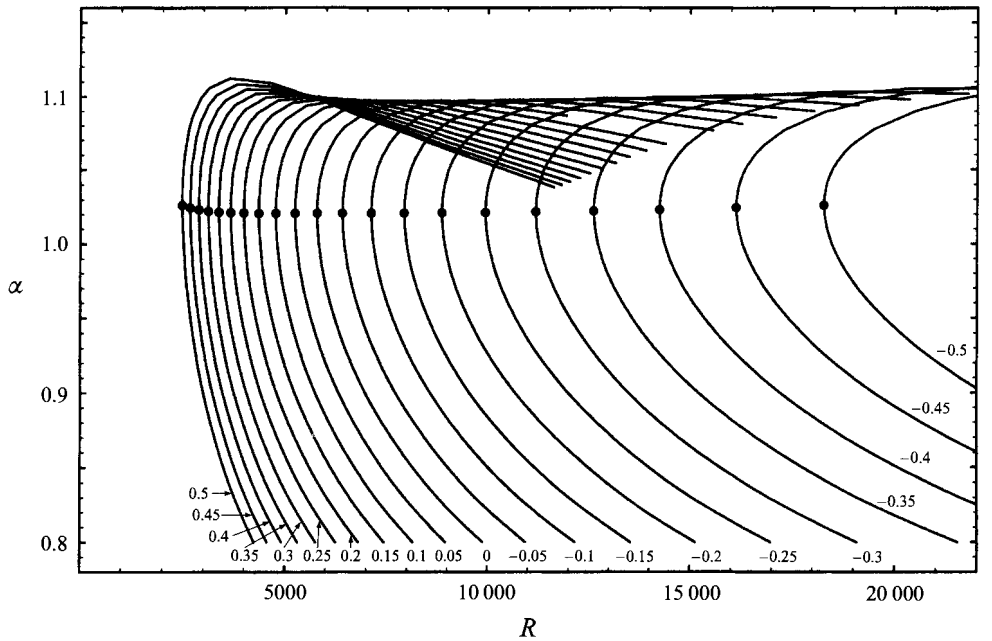

FIGURE 3. Marginal stability curves when $P_e = 1$ and $\mu(T) = e^{-K_1 T}$ for the values of K_1 indicated. On each curve the location of the critical point is shown by a dot.

6.1. *Model 1*

Figure 3 shows a selection of marginal stability curves calculated using the exponential viscosity/temperature relationship given by equation (3.5) for various values of K_1 when $P_e = 1$. In figure 4 we plot $R_c - R_c^0$, $\alpha_c - \alpha_c^0$ and $\sigma_c - \sigma_c^0$ against K_1. It can be seen that R_c decreases monotonically with K_1 and we may thus conclude that the effect of heating the channel walls is always stabilizing if $K_1 < 0$, and is always destabilizing if $K_1 > 0$. The calculations also show that α_c^0 is the global minimum value of α_c and that σ_c is a monotonically increasing function of K_1. Figure 5 shows the critical eigenfunctions ψ and T for various values of K_1 when $P_e = 1$, where we have normalized the eigenfunctions by setting $\psi_r(0) = 1$. Clearly symmetry is lost for non-zero K_1.

It has been proposed that a mechanism for the instability of viscous channel flows is provided by the transfer of energy from the basic state to the disturbance via the Reynolds stress, S. In figure 6 we plot the critical Reynolds stress across the channel together with the location of the critical layers for various values of K_1 when $P_e = 1$, where in the present study we define

$$S = \psi_r \frac{d\psi_i}{dy} - \psi_i \frac{d\psi_r}{dy}. \tag{6.1}$$

When $K_1 > 0$ the critical layer nearest the cold wall shifts towards the centre of the channel while the other critical layer shifts closer to the hot wall. This behaviour is reversed when $K_1 < 0$. The Reynolds stresses peak close to the location of the critical layers in each case, suggesting that the instability mechanism is similar to that of the isothermal problem (the plot for $K_1 = 0$ in figure 6). We note, however, that the Reynolds stresses near the hot-wall critical layer are clearly more important than those near the cold-wall critical layer when $K_1 > 0$ and *vice versa*.

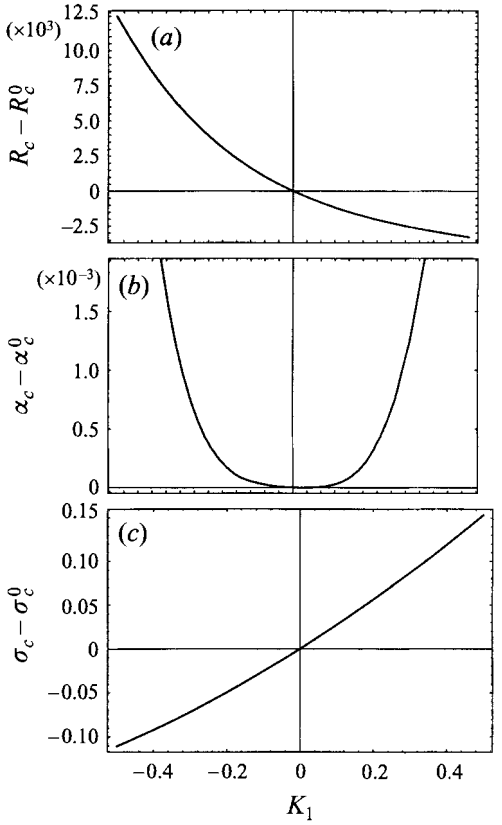

FIGURE 4. (*a*) $R_c - R_c^0$, (*b*) $\alpha_c - \alpha_c^0$, (*c*) $\sigma_c - \sigma_c^0$ plotted as functions of K_1 for $\mu(T) = \mathrm{e}^{-K_1 T}$ when $P_e = 1$.

6.2. *Model 2*

Figure 7 shows a selection of marginal stability curves calculated using the linear viscosity/temperature relationship given by equation (3.7) for various values of K_2 when $P_e = 1$. Figure 7 shows that the stability behaviour for this model is somewhat more complicated than for model 1. This is further illustrated in figure 8, where we plot the values of $R_c - R_c^0$, $\alpha_c - \alpha_c^0$ and $\sigma_c - \sigma_c^0$ against K_2. Evidently R_c increases monotonically as K_2 decreases from zero as before. However, as K_2 increases from zero, R_c initially decreases, before reaching a global minimum and subsequently increasing monotonically, with our results suggesting that $R_c \to \infty$ as $K_2 \to 1/2$. Thus the flow may be arbitrarily stabilized not only by making the magnitude of $K_2 < 0$ sufficiently large, but also by allowing K_2 to approach sufficiently close to $1/2$. For any P_e we can identify a global critical Reynolds number, $R_c^*(P_e)$, with a corresponding global critical wavenumber $\alpha_c^*(P_e)$ and wave speed $\sigma_c^*(P_e)$, which occurs at the value $K_2 = K_{2c}^*(P_e)$, for which any flow with $R < R_c^*$ is stable to any disturbance for any value of K_2 and for which any flow with $R > R_c^*$ will be unstable to some disturbances for some values of K_2. Typical values of R_c^*, α_c^*, σ_c^* and K_{2c}^* for various values of P_e are tabulated in table 2, and in figure 9 we plot R_c^*, K_{2c}^*, α_c^* and σ_c^* against $\log_{10}(P_e)$; there appears to be no simple relationship of the global critical point with the value of P_e. For each value of P_e we can identify a value of K_2 which yields the same critical Reynolds number as the isothermal case: for instance if $P_e = 1$ then

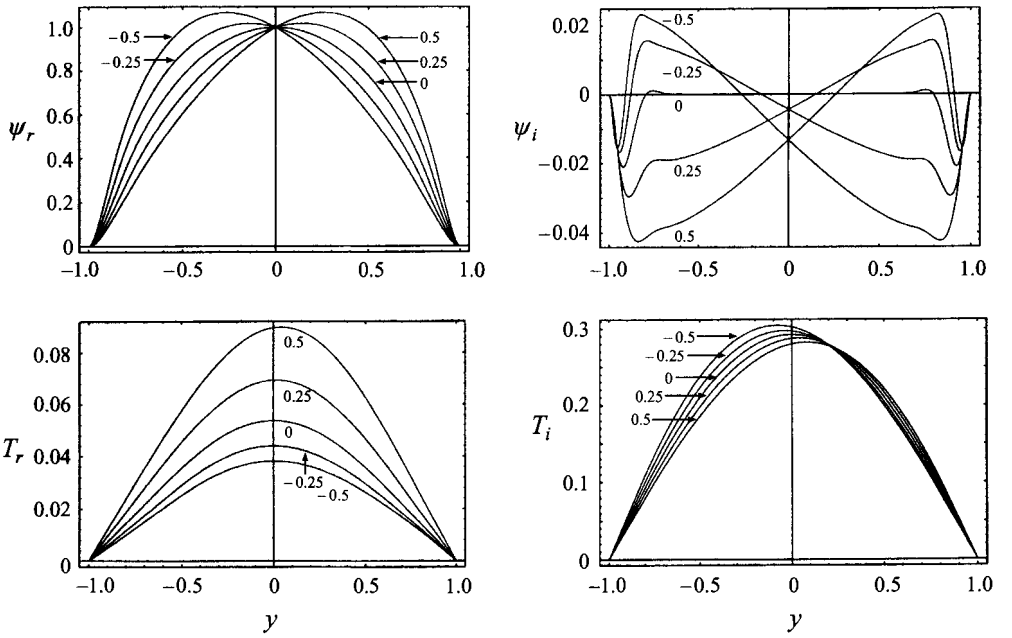

FIGURE 5. Critical eigenfunctions ψ and T for $\mu(T) = e^{-K_1 T}$ when $K_1 = -0.5, -0.25, 0, 0.25, 0.5$ and $P_e = 1$.

P_e	K_{2c}^*	R_c^*	α_c^*	σ_c^*
0	0.262	4049.3	0.9974	0.3414
10^{-3}	0.262	4049.3	0.9974	0.3414
10^{-2}	0.262	4049.3	0.9974	0.3414
10^{-1}	0.262	4049.5	0.9974	0.3414
1	0.262	4050.8	0.9975	0.3413
10	0.262	4047.8	0.9975	0.3415
10^2	0.262	4049.8	0.9974	0.3413
10^3	0.257	4106.9	0.9955	0.3385
10^4	0.255	4116.9	0.9963	0.3379
10^5	0.251	4131.2	0.9978	0.3369

TABLE 2. Values of K_{2c}^*, R_c^*, α_c^*, σ_c^* for the values of P_e indicated for $\mu(T) = 1 - K_2 T$. The calculations were made with $N = 120$ and $J = 14$. The values are accurate to the number of figures quoted.

$R_c \simeq R_c^0$ when $K_2 \simeq 0.4$, although the critical wave speed $\sigma_c \simeq 0.367$ is higher and the critical wavenumber $\alpha_c \simeq 0.97$ is smaller than in the isothermal case. Figure 10 shows the critical Reynolds stress across the channel together with the location of the critical layers for various values of K_2 when $P_e = 1$. The variation of the Reynolds stresses with K_2 is qualitatively similar to that described in the previous section. Note that the critical Reynolds stresses corresponding to $K_2 = 0$ and $K_2 = 0.4$ are quite different.

6.3. *Model 3*

Figure 11 shows $R_c - R_c^0$, $\alpha_c - \alpha_c^0$ and $\sigma_c - \sigma_c^0$ plotted as functions of K_3 when $P_e = 1$. When $K_3 < 0$, figure 11 shows that while initially R_c increases monotonically as K_3 decreases from zero, a global maximum $R_c^{**}(P_e)$ is reached. Values of $R_c^{**}(P_e)$, together with the corresponding values K_{3c}^{**}, $\alpha_c^{**}(P_e)$ and $\sigma_c^{**}(P_e)$ for various values of P_e are

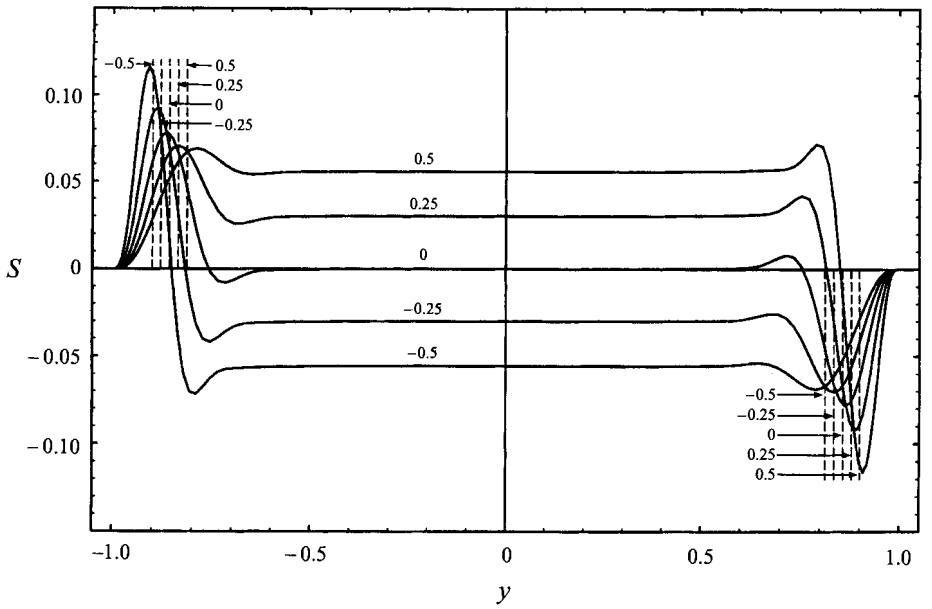

FIGURE 6. Critical Reynolds stress for $\mu(T) = e^{-K_1 T}$ when $K_1 = -0.5, -0.25, 0, 0.25, 0.5$ and $P_e = 1$. The location of the critical layers is shown by the dashed lines.

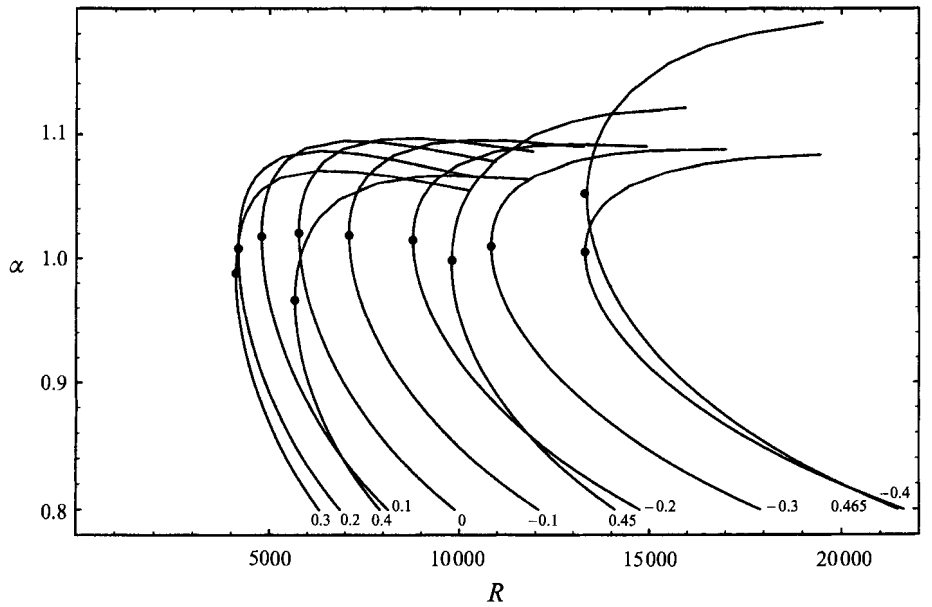

FIGURE 7. Marginal stability curves when $P_e = 1$ and $\mu(T) = 1 - K_2 T$ for the values of K_2 indicated. On each curve the location of the critical point is shown by a dot.

given by Wall (1996). Subsequently $R_c \to \check{R}_c(b)$ as $K_3 \to -\infty$ where $\check{R}_c(b) > R_c^0$. Since $\mu(T)$ tends uniformly to unity in the limit $b \to 0$ when $K_3 < 0$ we expect to recover $(R_c^0, \alpha_c^0, \sigma_c^0)$ in the limit $b \to 0$; this is confirmed by our numerical results given in table 3, where we tabulate $\check{R}_c(b)$ and the corresponding wavenumbers, $\check{\alpha}_c(b)$, and wave speeds, $\check{\sigma}_c(b)$, when $P_e = 1$. When $K_3 > 0$ the behaviour of the critical point

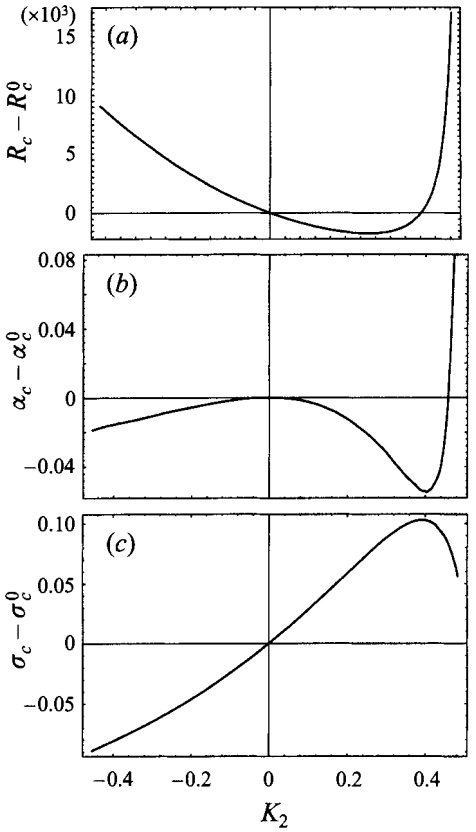

FIGURE 8. (*a*) $R_c - R_c^0$, (*b*) $\alpha_c - \alpha_c^0$, (*c*) $\sigma_c - \sigma_c^0$ plotted as functions of K_2 for $\mu(T) = 1 - K_2 T$ when $P_e = 1$.

is clearly similar to that of viscosity model 2 when $K_2 > 0$, with the flow arbitrarily stabilized as $K_3 \to \hat{K}_3$. When $K_3 > 0$, we may make $\mu(2)$ arbitrarily close to zero for any value of b by choosing K_3 sufficiently close to $\hat{K}_3$, so we would not necessarily expect to recover $(R_c^0, \alpha_c^0, \sigma_c^0)$ as $b \to 0$; our calculations demonstrate that this limit is singular. Similarly to viscosity model 2 we can identify a global critical Reynolds number $R_c^*(P_e)$ with corresponding values $\alpha_c^*(P_e)$, $\sigma_c^*(P_e)$ and $K_{3c}^*(P_e)$; values of these parameters for a range of values of P_e are also given by Wall (1996).

6.4. *Model 4*

Figure 12 shows $R_c - R_c^0$, $\alpha_c - \alpha_c^0$ and $\sigma_c - \sigma_c^0$ plotted as functions of K_4 when $P_e = 1$. Evidently R_c decreases monotonically as K_4 increases so that $K_4 > 0$ always destabilizes and $K_4 < 0$ always stabilizes the flow. The calculations also show that α_c^0 is the global minimum value of α_c and that σ_c is a monotonically increasing function of K_4 and so qualitatively the critical behaviour of this model is the same as that of model 1.

7. Comparison between the viscosity models

As we have seen, there are significantly different critical-point stability behaviours for the four different viscosity models when K_1, K_2, K_3, $K_4 > 0$, even though all

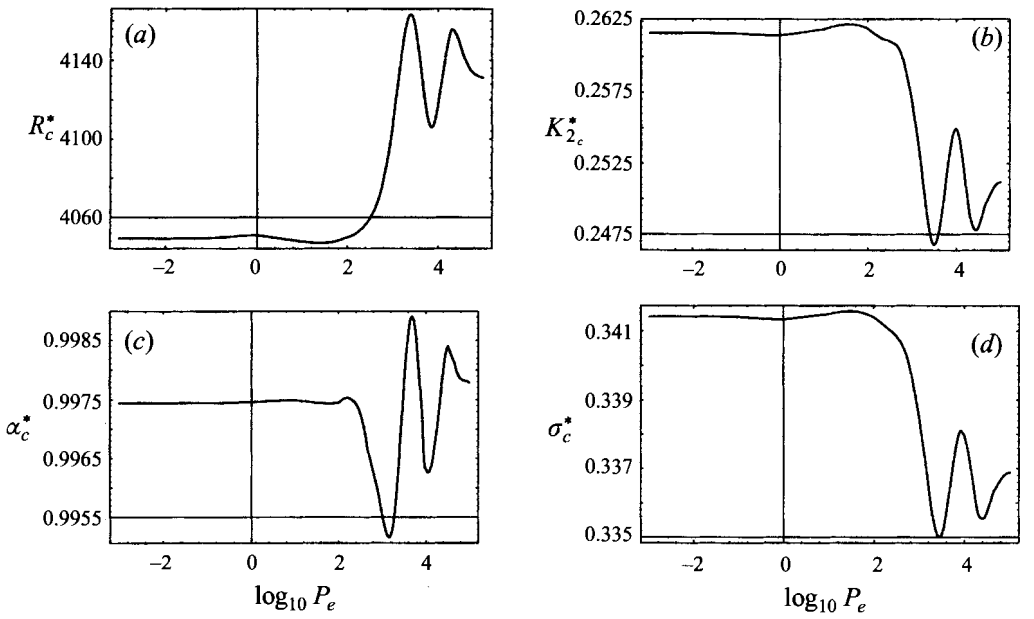

FIGURE 9. (a) R_c^*, (b) K_{2c}^*, (c) α_c^*, (d) σ_c^* plotted as functions of $\log_{10}(P_e)$ for $\mu(T) = 1 - K_2 T$.

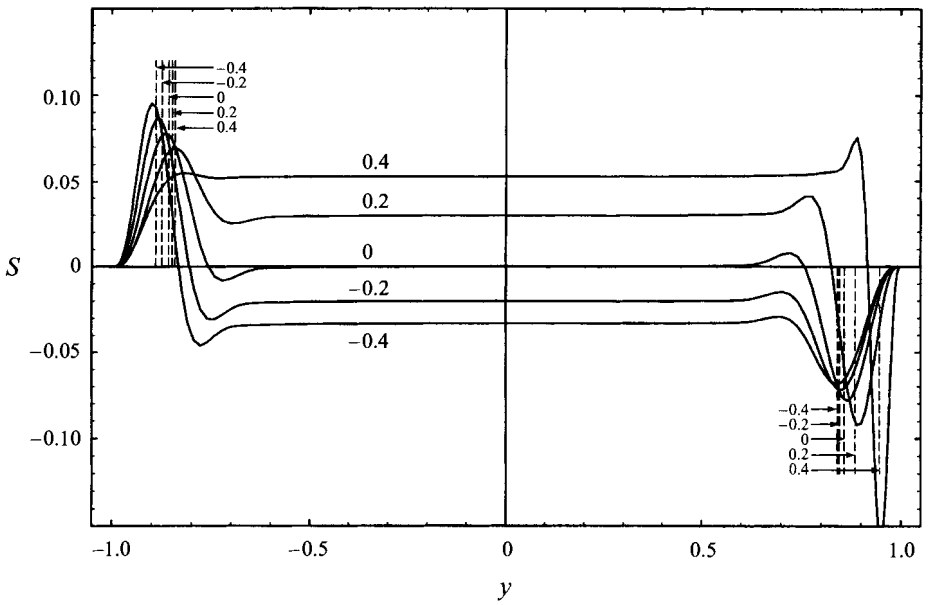

FIGURE 10. Critical Reynolds stress for $\mu(T) = 1 - K_2 T$ when $K_2 = -0.2$, 0, 0.2, 0.4 and $P_e = 1$. The location of the critical layers is shown by the dashed lines.

the viscosity relationships satisfy $\mu(0) = 1$, have $\mu(T) > 0$ everywhere in the channel and are monotonically decreasing functions of temperature. In order to compare the stability behaviour of all the viscosity models considered here we choose K_1, K_2, K_3, and K_4 so that $\mu'(0)$ agrees for the same values of the scaled parameters. Accordingly in figure 13 we plot $R_c - R_c^0$, $\alpha_c - \alpha_c^0$ and $\sigma_c - \sigma_c^0$ against $K_0 = K_1 = K_2 = bK_3 = K_4/F^2$.

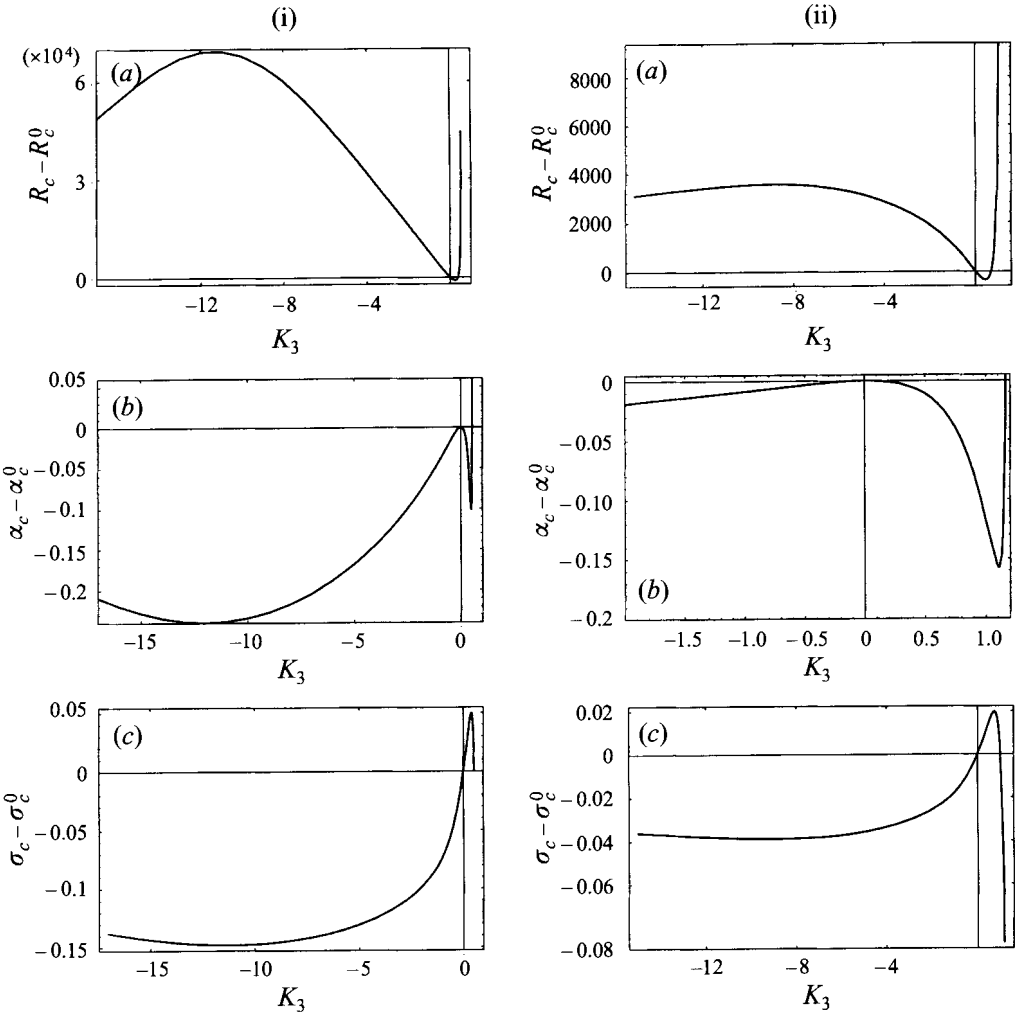

FIGURE 11(*a–c*) (i), (ii). For caption see next page.

In order to facilitate comparison with Schäfer & Herwig (1993) the Reynolds number used in figure 13(*a*) is one based on flux, that is a Reynolds number based on the velocity scale V_f defined in equation (2.3). We note that for a given $K_0 > 0$ the viscosity profiles for the various models are quite different: in particular for both viscosity models 1 and 4, as K_1 and K_4 respectively increase viscosity falls sharply near the cool wall ($y = -1$) and declines slowly throughout the rest of the channel creating a relatively viscous boundary layer near this wall relative to the rest of the channel. Contrastingly, with viscosity models 2 and 3 as $K_2 \to 1/2$ and $K_3 \to \hat{K}_3$ respectively a relatively less viscous layer of fluid forms near the hot wall ($y = 1$), though there must of course also be an inner viscous boundary layer in order that the no-slip condition can be satisfied. Confirmation that the value of the viscosity at the hot wall is not sufficient by itself to determine whether we observe the stabilizing behaviour associated with models 2 and 3 is given for example by comparing results for viscosity model 1 with $K_1 = 0.8304$ for which $\mu(2) = 0.19$ and $R_c = 1515 < R_c^0$ with those of viscosity model 2 when $K_2 = 0.405$ for which $\mu(2) = 0.19$ and $R_c = 5888 > R_c^0$. Figure 13 also demonstrates the singular nature of the limit $b \to 0$ since when $b = 0$ the problem reduces

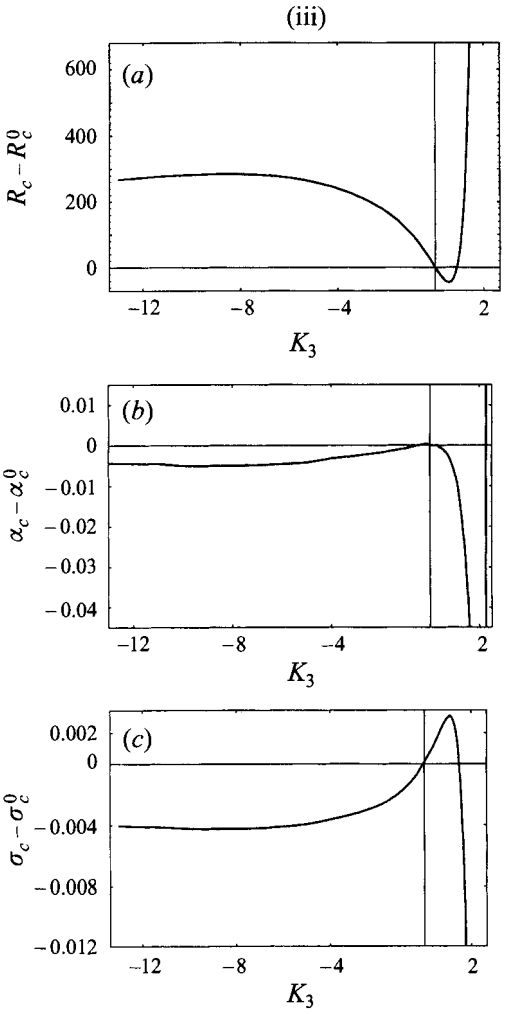

FIGURE 11. (*a*) $R_c - R_c^0$, (*b*) $\alpha_c - \alpha_c^0$, (*c*) $\sigma_c - \sigma_c^0$ plotted as functions of K_3 for $\mu(T) = 1 + b(1 - e^{K_3 T})$ for (i) $b = 0.5$, (ii) $b = 10^{-1}$, (iii) $b = 10^{-2}$ when $P_e = 1$.

to the isothermal Orr–Sommerfeld problem. In contrast, for all four viscosity models $R_c > R_c^0$ whenever $K_0 < 0$, though for models 1, 2 and 4 R_c increases monotonically as K_0 decreases whereas for model 3 R_c reaches a maximum R_c^{**} and subsequently tends to finite limit $\check{R}_c > R_c^0$ as $K_0 \to -\infty$. We note that, as expected, all the models agree at $K_0 = 0$, and for all models R_c and σ_c are monotonically decreasing and increasing functions of K_0 respectively in a neighbourhood of $K_0 = 0$, while, as is evident from figure 13(*b*), for viscosity models 1 and 4 the critical wavenumber α_c has a local minimum at $K_0 = 0$ whereas for models 2 and 3 it has a local maximum at $K_0 = 0$.

8. Comparison with Potter & Graber (1972)

In their study Potter & Graber (1972) simplified the eigenvalue problem posed by the differential equations (4.5) and (4.6) subject to (4.7) by omitting any perturbation to the basic-state temperature. This approximation is also used in more recent studies, see, for instance, the work of Pinarbasi & Liakopoulos (1995). This modified fourth-

b	$\check{R}_c(b)$	$\check{\alpha}_c(b)$	$\check{\sigma}_c(b)$
1	23086	1.02040	0.1321
0.5	12986	1.02048	0.1760
10^{-1}	6984	1.02051	0.2400
10^{-2}	5888	1.02055	0.2614
10^{-3}	5784	1.02055	0.2637
10^{-4}	5773	1.02055	0.2640
10^{-5}	5772	1.02055	0.2640

TABLE 3. Values of $\check{R}_c(b)$, $\check{\alpha}_c(b)$ and $\check{\sigma}_c(b)$ for various values of b when $P_e = 1$.

order Orr–Sommerfeld eigenvalue problem is recovered by setting $T \equiv 0$ in equation (4.5) and the boundary conditions (4.7). Note that P_e is therefore not a parameter of Potter & Graber's problem. It has apparently not been previously noted that Potter & Graber's approximation is exact in the case $P_e = 0$, since in this case equation (4.6) becomes $T'' - \alpha^2 T = 0$ subject to $T(\pm 1) = 0$, which yields the unique solution $T \equiv 0$. However, when $P_e \neq 0$ then T is not identically zero and so Potter & Graber's approximation is not exact. Potter & Graber did not consider the case $K_4 < 0$, but did find that R_c was a monotonically decreasing function of K_4 when $K_4 > 0$.

We can assess the accuracy of Potter & Graber's numerical technique by setting $P_e = 0$ in the present numerical calculations, since in this case the present problem reduces to exactly that solved by the earlier authors. In comparing our results for R_c when $P_e = 0$ with Potter & Graber's we find that the results differ by up to 2%, a discrepancy which we must therefore attribute to Potter & Graber's numerical calculations being less accurate than those of the present study. For instance, they obtain $R_c = 7800, 4600, 3900$ for $K_4 = 0, 0.0154728, 0.0216620$ respectively, which when rescaled appropriately correspond to $R_c = 5850, 2105, 1516$ as compared with our corresponding results $R_c = 5772.2, 2135.5, 1515.8$. The accuracy of their approximation, as opposed to the accuracy of their numerical technique, may only be measured by comparing the approximate results thus obtained with solutions to the full problem. Accordingly we calculate the quantity

$$\frac{R_c(K_4, P_e) - R_c(K_4, P_e = 0)}{R_c(K_4, P_e = 0)} \tag{8.1}$$

for various values of P_e. The results of this investigation for viscosity model 4 are plotted in figure 14. Schäfer & Herwig (1993) found the neglect of temperature perturbations to be a good approximation for small $|K_4|$; the results shown in figure 14 confirm this result. Figure 14 also shows that there is no simple relationship between the error in using Potter & Graber's approximation and the value of P_e.

9. Comparison with Schäfer & Herwig (1993)

In their study Schäfer & Herwig (1993) considered equations (4.5) and (4.6) in the asymptotic limit $K_0 \to 0$ and solved the resulting leading- and first-order problems numerically. In figure 13(a) we have also plotted the results of Schäfer & Herwig taken from figure 7 of their paper and the corresponding results of the present calculations when $P_e = 1$. As expected all the models agree with Schäfer & Herwig's asymptotic results for sufficiently small values of $|K_0|$. Schäfer & Herwig concluded that R_c decreased monotonically with K_0 and this conclusion is confirmed by our

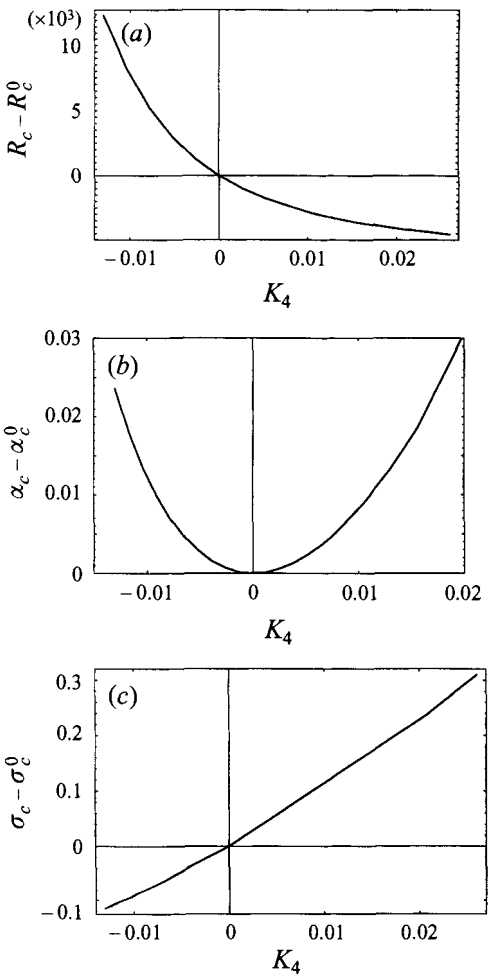

FIGURE 12. (*a*) $R_c - R_c^0$, (*b*) $\alpha_c - \alpha_c^0$, (*c*) $\sigma_c - \sigma_c^0$ plotted as functions of K_4 for $\mu(T) = Ce^{(K_4T+F)^{-1}}$ when $P_e = 1$.

non-asymptotic results provided that $|K_0|$ is sufficiently small. We observe that for $K_0 > 0$ the asymptotic results predict the flow to be less stable than any of our non-asymptotic results.

10. Discussion

In this study we have investigated the linear stability of parallel shear flow with temperature-dependent viscosity in a channel the walls of which are maintained at (different) constant temperatures. We considered four different viscosity models $\mu(T)$, where, depending on whether the parameter K_0 is positive or negative, $\mu(T)$ monotonically decreases or increases respectively as a function of temperature. The value $K_0 = 0$ corresponds to the isothermal Orr–Sommerfeld problem describing the linear stability of plane Poiseuille flow for which we obtained results which were in excellent agreement with those of previous authors. For the thermal problem the critical Reynolds number R_c depends both on K_0 and P_e. For all the viscosity models

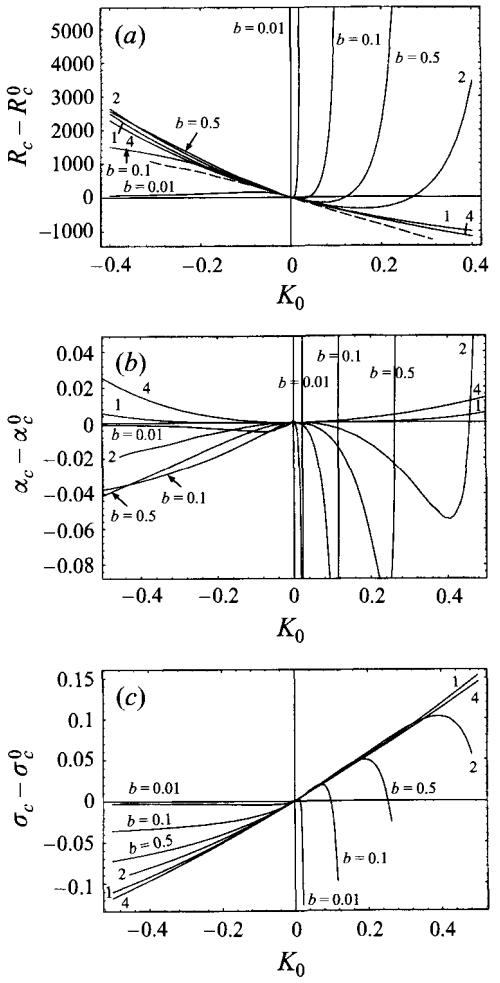

FIGURE 13. (*a*) $R_c - R_c^0$, (*b*) $\alpha_c - \alpha_c^0$, (*c*) $\sigma_c - \sigma_c^0$ plotted as functions of K_0 when $P_e = 1$ for the four different viscosity models. Schäfer & Herwig's (1993) asymptotic results are shown by the dashed line in (*a*).

considered here we found that R_c is a monotonically decreasing function of K_0 near $K_0 = 0$ in agreement with the asymptotic results of Schäfer & Herwig (1993). In most of the cases investigated R_c was a monotonically decreasing function of K_0 for a given P_e, the exceptions being viscosity model 3 for $K_0 < 0$, and viscosity models 2 and 3 for $K_0 > 0$. In the first case, $R_c > R_c^0$ attains a maximum for a finite negative value of K_0 and $R_c \to \check{R}_c$ as $K_0 \to -\infty$, where $\check{R}_c$ is finite. In the other cases a minimum value of $R_c < R_c^0$ is attained for a finite positive value of K_0 and subsequently $R_c \to \infty$ as K_0 approaches a finite limit. It may be noted that one consequence of this behaviour is the existence of a global critical Reynolds number, R_c^*, for models 2 and 3 for which fluids are stable to all disturbances for $R_c < R_c^*$.

The distribution of Reynolds stresses across the channel for the flows considered in this study have been shown to be similar to the isothermal problem in so far as there are peaks in these stresses near both the critical layers, and the stability mechanisms of these flows are therefore expected to be similar to those of plane Poiseuille flow. However, when K_0 is non-zero the flow skews towards one side of the channel and

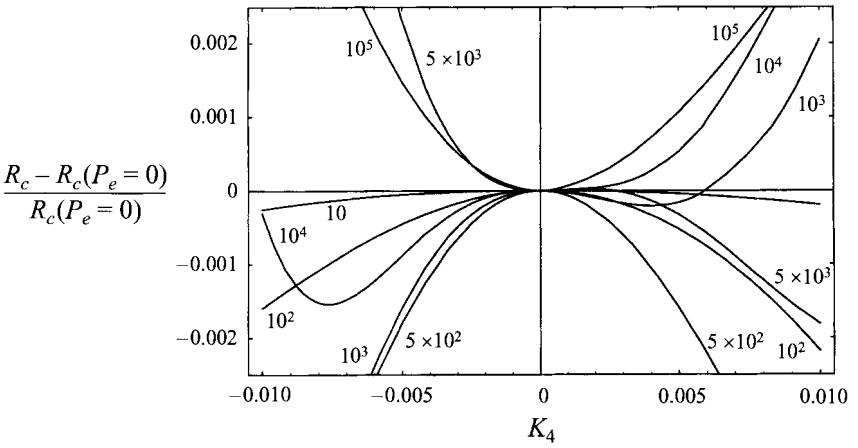

FIGURE 14. $(R_c - R_c(P_e = 0))/R_c(P_e = 0)$ plotted as a function of K_4 for the values of P_e indicated for $\mu(T) = Ce^{(K_4T+F)^{-1}}$.

the critical layer in this half of the channel shifts towards the nearest channel wall with the Reynolds stresses near this layer becoming larger in comparison to the other critical layer, which shifts towards the centre of the channel in most cases. Transfer of energy from the basic state to the disturbance will thus be greater in the half of the channel into which the flow has skewed.

We found that the stability characteristics of the flow are only weakly dependent on the value of P_e, and that in all the cases investigated changing the value of P_e by many orders of magnitude did not alter the qualitative stability characteristics of the flow; Schäfer & Herwig (1993) described the same behaviour for small $|K_0|$. We found the approximate solution obtained by Potter & Graber (1972) by neglecting perturbations to basic-state temperature to be exact in the case $P_e = 0$, but only approximately correct for non-zero values of P_e. However, the relative lack of sensitivity of the full solution's eigenvalues to changes in the value of P_e ensures that Potter & Graber's approximation is accurate over a wide range of values of P_e.

Our findings contain several unexpected results. For instance, we have a situation where one flow whose viscosity monotonically decreases across the channel is arbitrarily *destabilized* by heating whereas another flow whose viscosity monotonically decreases across the channel is found to be arbitrarily *stabilized* by heating. In the remainder of this paper we discuss our results in terms of three physical effects, namely bulk effects, velocity-profile shape effects and thin-layer effects.

Bulk effects concern the destabilization or stabilization that occurs in a flow when fluid viscosity is uniformly decreased or increased respectively. This destabilization or stabilization occurs since the Reynolds number of the flow is increased or decreased by a uniform decrease or increase in viscosity respectively. In the present problem when K_0 is positive or negative viscosity throughout the channel is non-uniformly decreased or increased respectively and so there is a bulk effect included within this change. Bulk effects alone would therefore imply a monotonic decreasing relationship of R_c with K_0 and so any exceptions to such a relationship must be due to other effects. Particularly surprising are those exceptions which occur when $K_0 > 0$ since in these cases the flow may be made arbitrarily more *stable* in comparison with the isothermal solution by *reducing* the viscosity of the fluid everywhere in the channel. The bulk effect is easily filtered out of our results by the introduction of a new

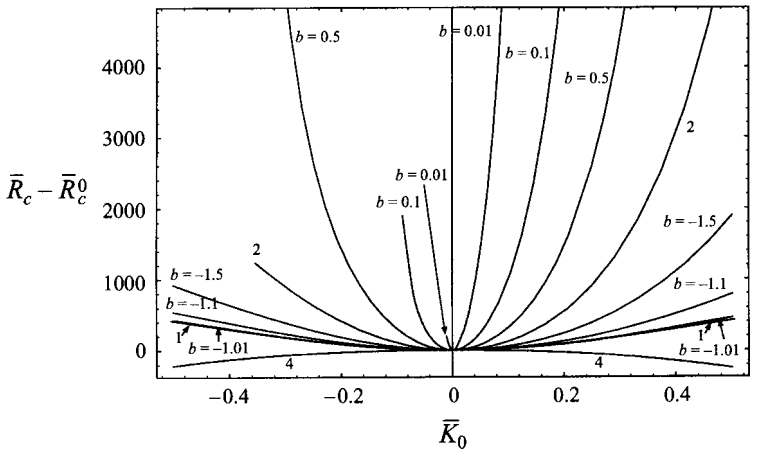

FIGURE 15. $\bar{R}_c - \bar{R}_c^0$ plotted as a function of $\bar{K}_0$ when $P_e = 1$ for the four different viscosity models.

Reynolds number, $\bar{R}_c$, based on average viscosity in the channel. If we also base the velocity scale given in equation (2.2) on average viscosity then

$$\bar{R}_c = \frac{R_c}{\left(\frac{1}{2}\int_0^2 \mu(T)\mathrm{d}T\right)^2}. \tag{10.1}$$

In figure 15 we plot $\bar{R}_c$ against $\bar{K}_0\,(= K_1)$ where values of $\bar{K}_0(K_i)$, $i = 2,\ldots,4$ for each value of K_i, $i = 2,\ldots,4$ are found such that

$$\int_0^2 \mu(T,\bar{K}_0(K_i))\mathrm{d}T = \int_0^2 \mathrm{e}^{-\bar{K}_0 T}\mathrm{d}T, \tag{10.2}$$

that is for a given value of $\bar{K}_0$ the average viscosity of all models is the same.† Evidently all the $\bar{R}_c$ curves are flat in the neighbourhood of $\bar{K}_0 = 0$ which suggests that bulk effects predominate in the limit $\bar{K}_0 \to 0$.

A second effect relevant to the present study is the stabilization which occurs when a symmetric basic-state velocity profile becomes skewed. Two notable studies of such a phenomenon are those by Potter & Smith (1968) and Mott & Joseph (1968) who both found skewed profiles to be more stable than the symmetric Poiseuille profile in the isothermal Orr–Sommerfeld problem (though in this problem the skewed profiles are not strictly solutions of the governing equations). For instance, Potter & Smith found that their critical Reynolds number based on average velocity increased from 3850 for the Poiseuille profile to 12100 for a quintic-polynomial skewed profile. This shape effect is thus stabilizing for both for positive and negative K_0.

A third effect relevant to the present study is that related to the formation of thin layers of fluid near a channel wall of differing viscosity relative to the fluid in the rest of the channel. Note that while there are many studies of 'thin-layer' effects which arise from consideration of the linear stability of the steady, cocurrent

† Obviously we cannot compare all the models for certain values of $\bar{K}_0$, for instance for model 3 we have $1 < \bar{\mu}(T) < 1 + b$ when $K_3 < 0$ so we cannot compare results obtained from viscosity model 3 for values of $\bar{K}_0 < \bar{K}_{0p}$ where $\bar{K}_{0p}$ is the solution to $1 + b = \frac{1}{2}\int_0^2 \mathrm{e}^{-\bar{K}_{0p}T}\mathrm{d}T$. Similar bounds exist for viscosity models 2 and 3 when $\bar{K}_0 > 0$.

parallel flow of two immiscible fluids any stability phenomena that rely essentially on the presence of an interface between the two fluids will clearly not be relevant to the present problem. Renardy (1987) investigated the linear stability of Poiseuille flow of one fluid encapsulated by a layer of a second fluid next to either wall and made a distinction between eigenvalues that branch from eigenvalues of the corresponding one-fluid problem (the linear stability of plane Poiseuille flow) labelled 'one-fluid' modes, and those that arise from the presence of the interfaces. She found that the addition of sufficiently thin layers of less-viscous fluid near both walls encapsulating the more-viscous core stabilizes the critical one-fluid mode. Renardy & Joseph (1985) considered the problem of the Couette flow of two fluids (in just two layers) between concentric cylinders and also presented results for one-fluid modes. They found that adding a sufficiently thin layer of less-viscous fluid adjacent to the inner (rotating) cylinder stabilizes these modes whereas adding a sufficiently thin layer of more-viscous fluid adjacent to the inner cylinder destabilizes them. Hooper (1989) considered a configuration consisting of two fluids in just two layers in plane Poiseuille flow. She found that a thin layer of less-viscous fluid adjacent to one of the channel walls destabilizes the one-fluid mode. For viscosity models 2 and 3 the shape of the viscosity profiles as $K_0 \to 1/2$ and $K_0 \to \hat{K}_0$ respectively, together with the corresponding behaviour of R_c suggests that the formation of a thin layer of fluid of differing viscosity to the fluid in the rest of the channel may have an important influence upon stability. However, the present results suggest that the formation of a thin layer of less-viscous fluid adjacent to a channel wall stabilizes the flow for the present problem and *vice versa*, so the 'thin-layer' effect described above appears to be quite different from those observed in the two-fluid problems.

To illustrate the above effects in relation to the present problem we consider the behaviour of R_c and $\overline{R}_c$ with K_0 and $\overline{K_0}$ respectively for viscosity model 3. Further discussion of the relation of these physical effects to the stability behaviour associated with the other viscosity models may be found in Wall (1996). If we consider the region $K_3 > 0$, the bulk effect is destabilizing while the shape effect is stabilizing. Figure 13(*a*) demonstrates that, as for all our results, the bulk effect dominates for sufficiently small K_3. However, figure 2 shows that in the limit $K_3 \to \hat{K}_3$ a thin layer of fluid forms next to the hot wall which is less viscous than the fluid in the rest of the channel. We tentatively attribute the unexpected stabilization that occurs in this limit to the formation of this less-viscous thin layer of fluid. We note that as $K_3 \to \hat{K}_3$ the viscosity in this layer becomes increasingly small which, we suggest, causes the stabilization due to the presence of the thin layer to become arbitrarily large. In contrast, the destabilization caused by the bulk effect is bounded since

$$1 + b - [\log(1 + 1/b)]^{-1} < \bar{\mu} < 1$$

when $b > 0$ and $0 < K_3 < \hat{K}_3$ (or when $b < -1$ and $\hat{K}_3 < K_3 < 0$), which may account for the overall arbitrary stabilization even when bulk effects are included. In contrast, the bulk effect for viscosity models 1 and 4 (and viscosity model 3 when $-1 < b < 0$) becomes arbitrarily destabilizing as $K_0 \to \infty$. For reference we also plot values of $\overline{R_c}$ corresponding to various values of $b < -1$ in figure 15. For $b < -1$ we require $K_3 > \hat{K}_3$ (for $b < 0$ the case $K_3 < 0$ corresponds to viscosity monotonically decreasing with temperature) and we again suggest that the less-viscous layer near the hot wall may be made arbitrarily stabilizing by choosing K_3 sufficiently close to $\hat{K}_3$. However, as may be seen from figure 2, the thin layer adjacent to the hot wall is not as well defined as those occurring for $b > 0$ and consequently stabilization of

bulk effects occurs for K_3 closer to $\hat{K}_3$. For example, in terms of K_0 we have $R_c = R_c^0$ for $K_0/\hat{K}_0 \approx 0.39$ when $b = 0.01$, 0.57 ($b = 0.1$), 0.69 ($b = 0.5$), 0.93 ($b = -1.5$) and 0.996 ($b = -1.1$). When $K_3 < 0$ and $b > 0$ both the bulk effect and the shape effect are always stabilizing when $|K_3|$ is finite. As K_3 decreases a thin layer of less-viscous fluid relative to the rest of the channel is formed near the cold wall which again we suggest is stabilizing. However, on this occasion the width of the layer tends to zero as $K_3 \to -\infty$ since $\mu(T) \to 1+b$ as $K_3 \to -\infty$ for $T > 0$ with $\mu(0) = 1$ while the ratio of viscosity of fluid in the thin layer to the rest of the channel is bounded between unity and $1+b$. We would therefore argue that the thin layer on this occasion reaches a maximum at a finite value of $K_3 < 0$, and thence becomes negligible as $K_3 \to -\infty$. Furthermore, as shown in equation (3.12), for viscosity model 3 the velocity profiles are symmetrical in the limit $K_3 \to -\infty$ and so the stabilizing shape effect also reaches a maximum for finite $K_3 < 0$ and eventually becomes negligible in the limit $K_3 \to -\infty$. Taken together, these effects would thus seem to offer a plausible explanation for why a maximum in $R_c = R_c^{**}$ occurs at finite $K_3 = K_{3c}^{**} < 0$ and thence R_c subsequently tends to $\check{R}_c > R_c^0$ in the limit $K_3 \to -\infty$. Figure 15 demonstrates clearly that the stabilization for viscosity model 3 for $b > 0$ as $K_3 \to -\infty$ is entirely due to bulk effects since $\overline{R}_c \to \overline{R}_c^0$ in this limit, furthermore we note the values of $\check{R}_c$ given in table 3 are given by $\check{R}_c = (1+b)R_c^0$ which is due entirely to the bulk effect since $\mu(T) \to 1+b$ for all $T > 0$ in the limit as $K_3 \to -\infty$.

Finally, we note that when $b = -1$ viscosity models 1 and 3 are identical (with $K_1 = -K_3$) and figure 15 demonstrates that the results for model 1 may be obtained from model 3 in the limit $b \to -1^-$. Furthermore, it may be noted that, in terms of K_0, viscosity model 3 is given by

$$\mu(T) = 1 + b(1 - \mathrm{e}^{K_0 T/b}) = 1 - K_0 T + O\left(\frac{1}{b}\right), \tag{10.3}$$

so $\lim_{b\to\pm\infty} \mu(T) = 1 - K_0 T$, and viscosity model 2 may be recovered as a limiting case of viscosity model 3 in the limit $b \to \pm\infty$.

One of the authors (D.P.W.) gratefully acknowledges the financial support of British Nuclear Fuels Ltd via a studentship.

REFERENCES

BRENT, R. P. 1973 *Algorithms for Minimization without Derivatives.* Prentice-Hall.

DRAZIN, P. G. & REID, W. H. 1981 *Hydrodynamic Stability.* Cambridge University Press.

FORNBERG, B. 1988 Generation of finite difference formulas on arbitrarily space grids. *Math. Comput.* **51**, 699–706.

GARY, J. & HELGASON, R. 1970 A matrix method for ordinary differential eigenvalue problems. *J. Comput. Phys.* **5**, 169–187.

GROSCH, C. E. & SALWEN, H. 1968 The stability of steady and time-dependent plane Poiseuille flow. *J. Fluid Mech.* **34**, 177–205.

HEISENBERG, W. 1924 Über Stabilität und Turbulenz von Flussigkeitsströmen. *Ann. Phys. Lpz.* **74** (4), 577–627.

HOOPER, A. P. 1989 The stability of two superposed viscous fluids in a channel. *Phys. Fluids* A **1**, 1133–1142.

KAPLAN, R. E. 1964 The stability of laminar incompressible boundary layers in the presence of compliant boundaries. *Aeroelastic and Structures Research Laboratory, Tech. Rep.* ASRLTR 166-1. Massachusetts Institute of Technology.

LAKIN, W. D., NG, B. S. & REID, W. H. 1978 Approximations to the eigenvalue relation for the Orr–Sommerfeld problem. *Phil. Trans. R. Soc. Lond.* A **268**, 325–349.

LIN, C. C. 1945*a* On the stability of two-dimensional parallel flow, Part I. *Q. Appl. Maths* **3**, 117–142.

LIN, C. C. 1945*b* On the stability of two-dimensional parallel flow, Part II. *Q. Appl. Maths* **3**, 218–234.

MOTT, J. E. & JOSEPH, D. D. 1968 Stability of parallel flow between concentric cylinders. *Phys. Fluids* **11**, 2065–2073.

NG, B. S. 1977 Approximations to the eigenvalue relation relation for the Orr–Sommerfeld problem: Numerical results for plane Poiseuille flow. *Tech. Rep.* FDL-77-011. Indiana University-Purdue University, Indianapolis.

ORR, W. 1907 The stability or instability of the steady motions of a perfect liquid and of a viscous liquid. *Proc. R. Irish Acad.* A **27**, 9–138.

ORSZAG, S. A. 1971 Accurate solution of the Orr–Sommerfeld stability equation. *J. Fluid Mech.* **50**, 689–703.

PINARBASI, A. & LIAKOPOULOS, A. 1995 The effect of variable viscosity on the interfacial stability of two-layer Poiseuille flow. *Phys. Fluids* **7**, 1318–1324.

POTTER, M. C. & GRABER, E. 1972 Stability of plane Poiseuille flow with heat transfer. *Phys. Fluids* **15**, 387–391.

POTTER, M. C. & SMITH, M. C. 1968 Stability of an unsymmetrical plane flow. *Phys. Fluids* **11**, 2763–2764.

RENARDY, Y. 1987 Viscosity and density stratification in vertical Poiseuille flow. *Phys. Fluids* **30**, 1638–1648.

RENARDY, Y. & JOSEPH, D. D. 1985 Couette flow of two fluids between concentric cylinders. *J. Fluid Mech.* **150**, 381–394.

SCHÄFER, P. & HERWIG, H. 1993 Stability of plane Poiseuille flow with temperature dependent viscosity. *Intl J. Heat Mass Transfer* **36**, 2441–2448.

SLOAN, D. M. 1977 Eigenfunctions of systems of linear ordinary differential equations with separated boundary conditions using Riccati transformations. *J. Comput. Phys.* **24**, 320–330.

SOMMERFELD, A. 1908 Ein Beitrag zur hydrodynamischen Erklaerung der turbulenten Fluessigkeits-bewegungen. *Proc. 4th Intl Cong. of Mathematicians* **III**, 116–124.

SQUIRE, H. B. 1933 On the stability for three-dimensional disturbances of viscous fluid flow between parallel walls. *Proc. R. Soc. Lond.* A **142**, 621–628.

TOLLMIEN, W. 1929 Über die Entstehung der Turbulenz. *Nachr. Ges. Wiss. Gottingen, Math.-Phys. Kl.*, 21–44.

TOLLMIEN, W. 1947 Asymptotische Integration der Störungsdifferentialgleichung ebener laminarer Strömungen bei hohen Reynoldschen Zahlen. *Z. Angew. Math. Mech.* **25/27** 33–50.

VINOKUR, M. 1983 On one-dimensional stretching functions for finite-difference calculations. *J. Comput. Phys.* **50** 215–234.

WALL, D. P. 1996 Thermal effects in fluid flow. PhD thesis, University of Strathclyde, Glasgow, UK.

WILKINSON, J. H. 1979 Kronecker's canonical form and the QZ algorithm. *Linear Algebra Appl.* **28**, 285–303.